Preprint
UCRL-JC-140161

Solar Opacities

B. F. Rozsnyai

This article was submitted to
9th international Workshop on Radiative Properties of Hot Dense Matter
Santa Barbara, CA
October 30 – November 3, 2000

October 4, 2000

U.S. Department of Energy
Lawrence
Livermore
National
Laboratory

Approved for public release; further dissemination unlimited

DISCLAIMER

This document was prepared as an account of work sponsored by an agency of the United States Government. Neither the United States Government nor the University of California nor any of their employees, makes any warranty, express or implied, or assumes any legal liability or responsibility for the accuracy, completeness, or usefulness of any information, apparatus, product, or process disclosed, or represents that its use would not infringe privately owned rights. Reference herein to any specific commercial product, process, or service by trade name, trademark, manufacturer, or otherwise, does not necessarily constitute or imply its endorsement, recommendation, or favoring by the United States Government or the University of California. The views and opinions of authors expressed herein do not necessarily state or reflect those of the United States Government or the University of California, and shall not be used for advertising or product endorsement purposes.

This is a preprint of a paper intended for publication in a journal or proceedings. Since changes may be made before publication, this preprint is made available with the understanding that it will not be cited or reproduced without the permission of the author.

This report has been reproduced
directly from the best available copy.

Available to DOE and DOE contractors from the
Office of Scientific and Technical Information
P.O. Box 62, Oak Ridge, TN 37831
Prices available from (423) 576-8401
http://apollo.osti.gov/bridge/

Available to the public from the
National Technical Information Service
U.S. Department of Commerce
5285 Port Royal Rd.,
Springfield, VA 22161
http://www.ntis.gov/

OR

Lawrence Livermore National Laboratory
Technical Information Department's Digital Library
http://www.llnl.gov/tid/Library.html

Solar Opacities.

Balazs F. Rozsnyai, L-023
Lawrence Livermore National Laboratory
P.O. Box 808
Livermore, California 94550

Abstract. Solar opacities are presented from the center of the Sun to the photosphere. The temperatures, densities and hydrogen mass fractions are taken from the standard solar model. For the heavy element abundances the Grevesse mixture is used. In the solar interior photoabsorption is dominated by free-free absorption and we compare two sets of opacities based on two different models for the inverse bremsstrahlung. The radiative luminosities calculated from the two sets of opacities are compared with those predicted by previous models of the standard solar model and also with the known luminosity of the Sun. Pressures, specific heats and the speed of sound in the solar plasma are also presented.

I. Introduction.

Solar opacities are key elements in understanding the physical processes in the interior of the Sun. They influence the details of the nuclear reactions, thus the solar neutrino flux, luminosity and whole array of physical details. In addition, the blossoming field of helioseismology provides a large array of accurately measured (between 0.01 and 0.04%) p-mode oscillation frequencies. Solar neutrinos and helioseismology are complimentary tools in studying solar structure. The effect of solar opacities on the standard solar models was investigated in the past [1,2], however, as the physical models of photoabsorption in hot plasmas become more sophisticated, it seem appropriate to re-calculate solar opacities. The word 'standard model' is frequently used throughout this paper and it is described in Refs. 1 and 2. In general, 'standard model' means the application of the best available physics to describe solar conditions. This paper focuses on solar opacities, however the quantum mechanical model upon which the opacities rest also provide some vital equation of state data. In Section II. We present a brief description of the of the quantum mechanical basis of the calculations and in Section III we present computed data.

II. Quantum mechanical basis of opacity calculation.

There are numerous publications about the details of opacity calculations. For a quick review of the current status of opacity models the reader is referred to the WorkOp-III:94 report of the Max-Planck Institut fur Quantenoptik[3]. Additional papers addressing the quantum mechanical details of hot plasmas together with the computation of photoabsorption were published elsewhere [4,5,6], here we only recall the essential elements.

The photoabsorption cross section in hot plasmas can be broken down into five components;

$$\sigma(h\nu) = \sigma^{bb}(h\nu) + \sigma^{bf}(h\nu) + \sigma^{ff}(h\nu) + \sigma^{sc}(h\nu) + \sigma^{pair}(h\nu) \qquad (1)$$

where the superscripts stand for the processes bound-bound, bound-free, free-free, scattering and pair production, respectively. In the solar interior he cross section is dominated by one ore more of the above components. In the interior, the photoabsorption is dominated by the free-free process, which is inverse bremsstrahlung, whereas in the outer regions where the heavy elements are only partially ionized, the bound-bound and bound-free processes are dominant. Scattering and pair production are important only at very high photon energies and they have insignificant roles.

The bound-bound or line cross sections usually involve a large number of spectral lines and they are given by

$$\sigma_{nl\to n'l'}(h\nu)=\frac{4\pi}{3}\alpha\sum_{P}W(P)p_{nl}(P)Av(n'l',P)h\nu\frac{l_{>}}{2l+1}Q^{2}(nl;n'l')b_{nl\to n'l'}(h\nu;P) \qquad (2)$$

In Equ.(2) nl→n'l' means a transition when an electron is elevated from a quantum level nl to n'l' in a certain many-electron configuration P. Equ.(2) can easily be generalized for j-j coupling. The number of nl→n'l' (or nlj→n'l'j' in j-j coupling) transitions can be very large due to the number of many-electron configurations. A major part of any opacity code is to obtain a sufficient number of many-electron configurations and the statistical distribution W(P). In Equ.(2) α stands for the fine structure constant, p_{nl} for the occupancy of the initial level, Av for the availability of the final level, hν for the photon energy, Q for the dipole transition integral and b for the line-shape function which is a crucially important element. Since Equ.(2) uses the distribution of the many-electron states, it is labeled as "detailed configuration accounting"(DCA). Details of computing line arrays can be found in refs. 5 and 6.

We note that the calculations presented here were done within the framework of the ion-sphere model. For each Z component a radius is given determined by the total plasma density and by the requirement that the electronic Fermi level for each Z component be the same. The number of electrons within the ion-sphere radius must be equal to Z, the nuclear charge, which assures charge neutrality within the ion-sphere.

Photoionization is analogous to the line transition except that the final state is in the continuum. There, the line shape function is replaced by the density of the final states. The computation of the density of the final states together with the proper normalization of the continuum wave functions are not entirely trivial, and they are not identical in the ion-sphere and in Debye-Huckel type models. In the ion-sphere model the density of states of an l partial wave in the WKB approximation is given by

$$\rho_l(\varepsilon)=\frac{1}{\pi}\int_{r_i}^{r_0}\left\{2\left[\varepsilon-V(r)\right]-\frac{(l+1/2)^2}{r^2}\right\}^{-1/2}dr \qquad (3)$$

where r_i and r_0 stand for the inner turning radius and the ion-sphere radius, respectively and ε is the continuum energy. If the radial wave function $R_{l,\varepsilon}(r)$ is normalized to unity within the ion-sphere, then the proper continuum wave function is

$$F_{l,\varepsilon}(r)=[\rho_l(\varepsilon)]^{1/2}R_{l,\varepsilon}(r) \qquad (4).$$

It is easy to show that in the limit when the ion-sphere goes to infinity, which is also the Debye-Huckel limit we have

$$\mathbf{F}_{l,\varepsilon}(\mathbf{r}) \rightarrow \left[\frac{2\mathbf{k}}{\pi}\right]^{1/2} \mathbf{j}_l(\mathbf{k}_\varepsilon \mathbf{r} - \delta_{l,\varepsilon}) \tag{5}$$

Where j stand for the spherical Bessel function, k for the wave vector and δ for the phase shift, respectively.

In the Debye-Huckel limit when $r_0 \rightarrow \infty$ the continuum wave functions given by Eq.(4) are normalized on the energy scale in the standard fashion as

$$\int_0^\infty \mathbf{F}_{l,\varepsilon}(\mathbf{r})\mathbf{F}_{l,\varepsilon'}\mathbf{r}^2\mathbf{dr} = \delta(\varepsilon - \varepsilon')$$

The photoionization process, just like the spectral line accounting, has to be done within the DCA approach with the net effect that the DCA approach predicts a set on nl photoionization edges in the vicinity of the average nl edge.

In the solar interior the dominant photoabsorption process is free-free absorption or inverse bremsstrahlung. Inverse bremsstrahlung is calculated by using Kramer's classical cross section multiplied by the so called free-free Gaunt factor which accounts for the quantum mechanical corrections. The cross section is given by

$$d\sigma^{ff}(h\nu) = \frac{16\pi}{3\sqrt{3}} Z^* e^4 \alpha \frac{1}{(h\nu)^3} g^{ff}(k_i k_f) f(\varepsilon_i) d\varepsilon_i \tag{6}$$

where f(ε) stands for the energy distribution of free electrons in the ion-sphere volume of the central ion and g for the free-free Gaunt factor, which is a function of the initial and final wave vector of the continuum electrons. In the low photon energy limit, which the most important in the case of inverse bremsstrahlung, the free-free Gaunt factor is given by [7]

$$g^{ff}(k_i k_f) = \frac{\sqrt{3}}{\pi} k_i k_f \sum_{l=0}^{\infty} (l+1) \sin^2[\delta_l(k) - \delta_{l+1}(k)] \tag{7}$$

A somewhat simpler approach to the free-free Gaunt factor is given by the Born-Elwert approximation [8]

$$\mathbf{g}^{ff}_{BE}(\mathbf{k}_i \mathbf{k}_f) = \frac{\sqrt{3}}{\pi} \frac{1}{Z^{*2}} \mathbf{I}(\mathbf{k}_i \mathbf{k}_f) \frac{\eta'}{\eta} \frac{1 - \exp(-2\pi\eta)}{1 - \exp(-2\pi\eta')} \tag{8}$$

where

$$\mathbf{I}(\mathbf{k}_i \mathbf{k}_f) = \frac{1}{e^4} \int_{k_i}^{k_f} [2\pi^2 \mathbf{V}(\mathbf{q})]^2 \mathbf{q}^3 \mathbf{dq} \tag{9}$$

and $\eta = \frac{Z^*}{k_i}$ and $\eta' = \frac{Z^*}{k_f}$

In Equ.(9) V(q) id the Fourier transform of the potential in which the free electrons move. For the scattering we use the Klein -Nishina formula and pair creation becomes important only above 1MeV photon energy.

This summarizes the theoretical background, in the next Section we present computational results.

III. Computations for the solar plasma.

The Sun consists mainly oh hydrogen and helium with traces of heavier elements up to Z=28. The heavier elements play a crucial role in the photoabsorption characteristics of the solar plasma, thus it is important to have a good idea about the heavy element abundances. There are at least three proposed heavy element distributions due to Grevesse [9], Aller[10] and Ross-Aller[11] and they are given in Table I, and a graphical illustration is shown in Fig. 1. In Fig. 1 the Grevesse and Aller distributions are hardly distinguishable, and the only visible difference in the Ross-Aller distribution is the reduction of the neon and argon components.

Table I. Fractional abundances of heavy elements in the Sun.

Element	Number fraction (Grevesse, 1984)	Number fraction (Aller, 1986)	Number fraction (Ross-Aller, 1976)
C	0.29661	0.27983	0.30279
N	0.05918	0.05846	0.06326
O	0.49226	0.49761	0.50249
Ne	0.06056	0.06869	0.02699
Na	0.00129	0.00125	0.00138
Mg	0.02302	0.02552	0.02892
Al	0.00179	0.00198	0.00241
Si	0.02149	0.02672	0.03244
P	0.00017	0.00018	0.00023
S	0.00982	0.01040	0.01151
Cl	0.00019	0.00019	0.00023
Ar	0.00230	0.00227	0.00073
Ca	0.00139	0.00134	0.00163
Ti	0.00006	0.00007	0.00008
Cr	0.00028	0.00035	0.00037
Mn	0.00017	0.00016	0.00019
Fe	0.02883	0.02382	0.02297
Ni	0.00108	0.00114	0.00138
Total	1.0000	1.0000	1.00000

To the heavy element distribution given by Table 1 the hydrogen and helium components have to be added and the number fractions must be properly renormalized. In the actual solar mixture we take one of the columns in Table 1, add the helium and hydrogen components in such a way that the mass fractions of the hydrogen, helium and heavy element components follow the prescription of the standard solar model. Customarily, the mass fractions of the hydrogen, helium and heavy elements are labeled by X, Y and Z, respectively. In this paper the calculations were done by using the Grevesse distribution with Z=0.0195. The hydrogen mass fraction X is a function of the solar radius due to the nuclear reactions in the center region. In Figures 2, 3 and 4 we show X, the solar density and temperature as a function of the solar radius. It should be noted that the presently accepted solar radius R_0 is 6.96 x10^{10} cm. The data shown in Figs. 2, 3 and 4 were taken from the standard model of

Ref. [1] and they are very close to that of the standard model of D. Dearborn [12]. Figure 5 shows the Rosseland mean opacity versus solar radius for the Grevesse mixture.
An important quantity is the radiative luminosity given by

$$L(r) = -4\pi r^2 \frac{4ca}{3\sigma_R \rho}(kT)^3 \frac{\partial(kT)}{\partial r} \tag{10}$$

where σ_R and ρ stand for the Roseland mean opacity and plasma density, respectively and $a = \frac{\pi^2}{15}\frac{1}{(\hbar c)^3}$. In Fig. 6 we show three luminosity curves, the solid curve is the total luminosity given by Dearborn [12] including convective luminosity, and the short dashed and long dashed curves are the radiative luminosities computed by the author. The short and long dashed curves correspond to the usage Eq.(7) and Eq.(9) for the free-free Gaunt factor, respectively.
In Figs. 7 and 8 we show some frequency dependent opacities of the solar mixture at different solar radii. We show the opacities at the center of the Sun corresponding to kT=1362.1 eV and 157.02 g/cc density, near half-way from the center at 0.5545 solar radius where the temperature and density are 293.24 eV and 0.7727 g/cc, respectively and in Fig. 8 we show the opacity near the photosphere at $r \approx R_0$, kT=1.0724 eV and 9.616×10^{-7} g/cc. As is evident from Figs. 7 and 8, as lower temperatures the spectral lines due to the heavy element components become more dominant.
Next, we investigate some of the equation-of state properties of the solar plasma In Figs. 9 and 10 we show the pressure and the specific heat C_V per particle (electrons and nuclei) as a function of the solar radius.
For helioseismology the speed of sound is important given by

$$C_s = \left[\gamma \left.\frac{\partial P}{\partial \rho}\right|_{kT}\right]^{1/2} = c\left[\gamma\left(1 + 2Z^* \frac{F_{1/2}(\eta)}{F_{-1/2}(\eta)}\right)\frac{kT}{Mc^2}\right]^{1/2} \tag{11}$$

where c stands for the velocity of light, kT and Mc^2 for the temperature and ionic mass in the same energy units, Z^* for the degree of ionization, γ for the ratio of the specific heats C_P/C_V, η for the degeneracy parameter of the electron gas and the F-s stand with the Fermi-Dirac integrals given by

$$F_n(\eta) = \int_0^\infty \frac{t^n dt}{\exp(t-\eta)+1}.$$

The specific heats are given by

$$C_V = \frac{3}{2} + C_V^{el} \quad \text{and} \quad C_P = \frac{5}{2} + C_P^{el}$$

where the superscript 'el' refers to the contribution from the plasma electrons. In this work for C_V^{el} and η we take the values as determined by the self consistent states of the Z components of the solar plasma. However, since the computation of C_P^{el} at present is not included in the self consistent procedure, for the later we take the value determined for a free electron gas,

$$C_p^{el} = C_v^{el} + Z * \frac{1}{3}\frac{F_{3/2}(\eta)}{F_{1/2}(\eta)}\left[\frac{5}{3}\frac{F_{3/2}(\eta)F_{-1/2}(\eta)}{F_{1/2}^2(\eta)} - 3\right] \tag{12}$$

In Fig. 11 we show the speed of sound as given by Eq.(11). Actually, Fig. 11 shows three barely distinguishable curves, the two solid lines are those of the author and D. Dearborn[12] and the dashed line is experimental, as provided to the author by D. Dearborn. The relative deviations in the three curves of Fig. 11 are les than .1%.

Conclusion.

The Sun is an excellent object to test the different parts of the physics of the solar model. The opacities and the equation-of state data are closely coupled to determine the equilibrium conditions of the Sun, thus the solar plasma is very good for testing theoretical models for radiative and equation-of state predictions. With new and more accurate observations solar physics will continue to play an active part in plasma research.

Acknowledgment.

This work was performed under the auspices of the U.S. Department of Energy by the University of California Lawrence Livermore National Laboratory under Contract No. W-7405-Eng-48.

References:

1 "Standard solar models and the uncertainties in predicted capture rates of solar neutrinos." John N. Bahcall, Walter F. Huebner, Stephen H. Lubow, Peter D. Parker and Roger K. Ulrich, Rev. Mod. Phys. **54,** 767 (1982).

2 "Solar models, neutrino experiments, and helioseismology." John N. Bahcall and Roger K. Ulrich, Rev. Mod. Phys. **60,** 297 (1988).

3 WorkOp-III:94, report MPQ 204, Max-Planck Institut Fur Quantenoptik, August 1995, edited by A.Rickert, K. Eidmann, J. Meyer-Ter-Vehn, F.J.D. Serduke and C.A. Iglesias.

4 B. F. Rozsnyai, Phys. Rev. **A5**, 1137 (1972).

5 A. Goldberg, B. F. Rozsnyai and P. Thompson, Phys. Rev. **A34**, 421 (1986).

6 B. F. Rozsnyai, S. D. Bloom and D. A. Resler, Phys. Rev. **A44**, 6791 (1991).

7 B. F. Rozsnyai and M. Lamoureux, JQSRT **43,** 381 (1990).

8 B. F. Rozsnyai, JQSRT **22,** 337 (1979).

9 N. Grevesse, Phys.Scr. **T8**, 49 (1984).

10 L. H. Aller, *Spectroscopy of Astrophysical Plasmas,* edited by A. Dalgarno and D. Layzer, (Cambridge University Press, Cambridge, England), p 89.

11 J. E. Ross and L. H. Aller, Science **191**, 1223 (1976).

12 D. M. Dearborn, Lawrence Livermore National Laboratory, private communication.

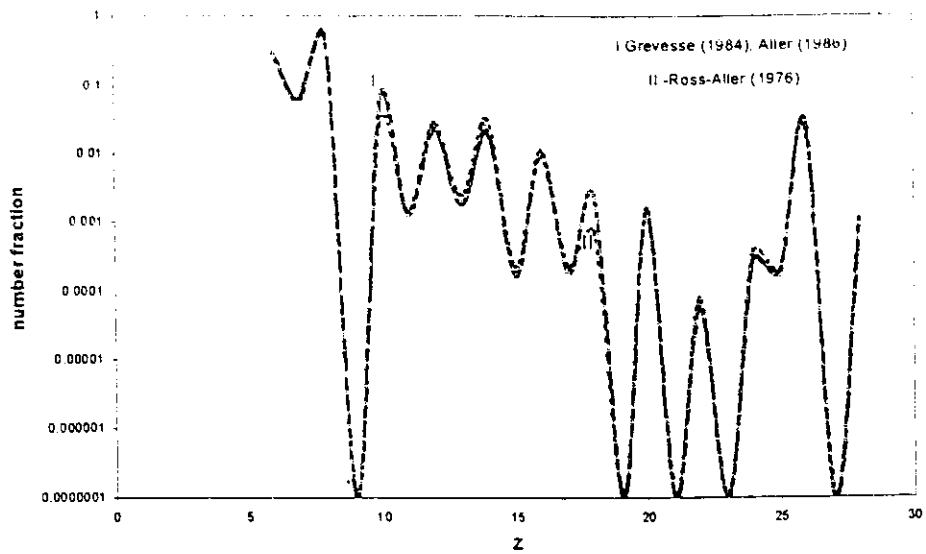

Fig. 1. Heavy element (Z>2) distribution in the solar plasma. Calculations in this paper were done for the Grevesse mixture.

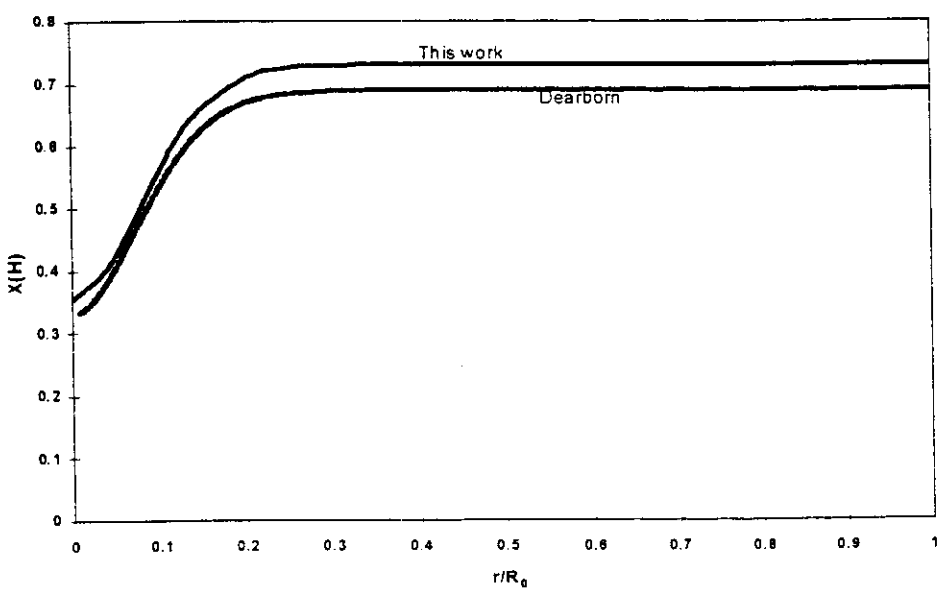

Fig. 2. Hydrogen mass fraction versus solar radius as determined by the standard model.

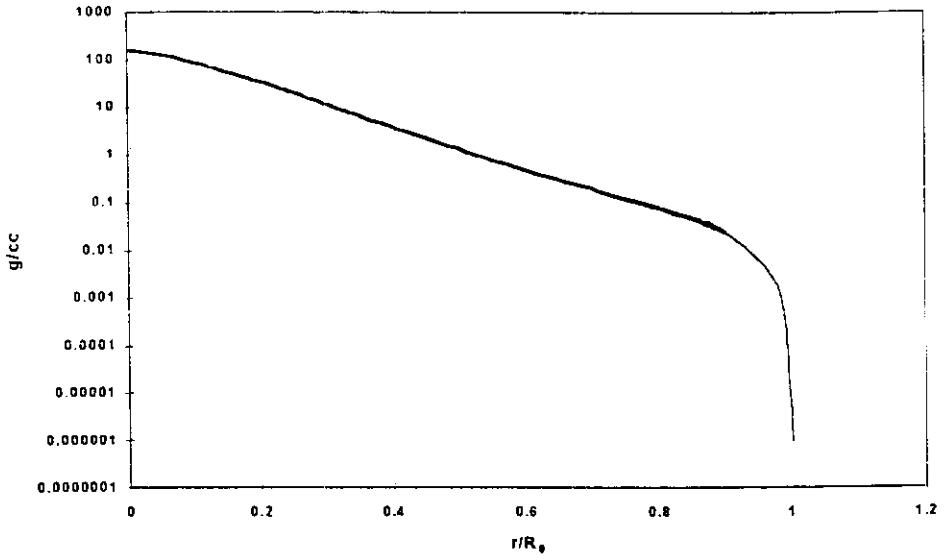

Fig. 3. Density of the solar plasma versus solar radius. The thick line is given by the standard model, the extended thin line extension is this work.

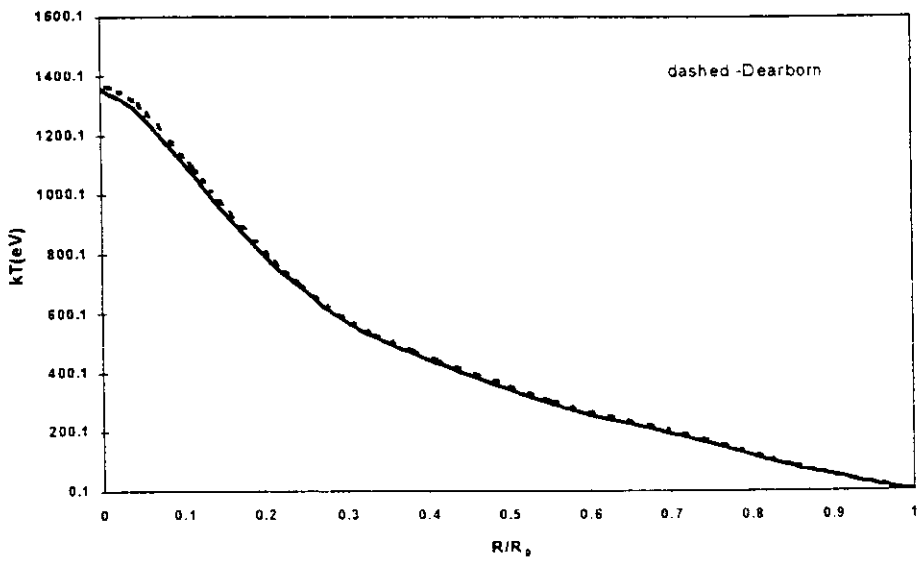

Fig. 4. Solar temperature versus solar radius. The dashed line is given by the standard model.

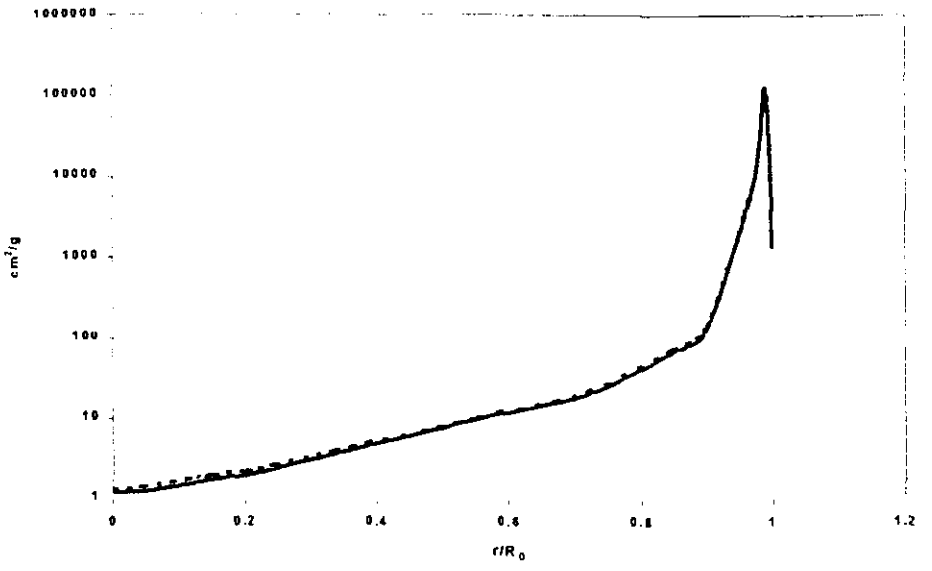

Fig. 5. Rosseland mean opacity of the solar plasma versus solar radius. The solid and dashed curves correspond to Eq.(7) and Eq.(8) for the free -free Gaunt factor, respectively.

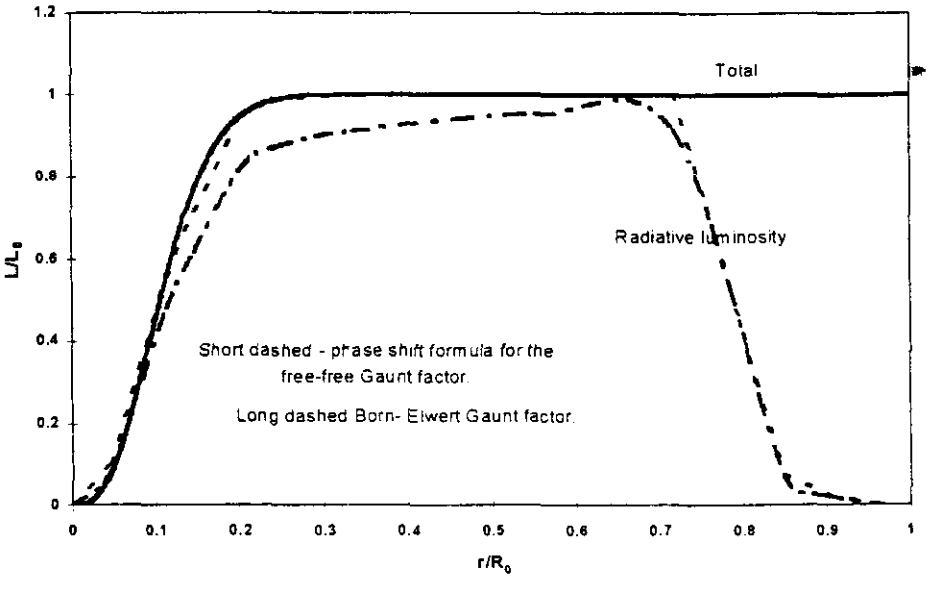

Fig. 6. Solar luminosities versus solar radius. The solid curve is given by the standard model and includes the convective luminosity. The dashed curves are radiative luminosities calculated in this work with the two forms of the free -free Gaunt factor.

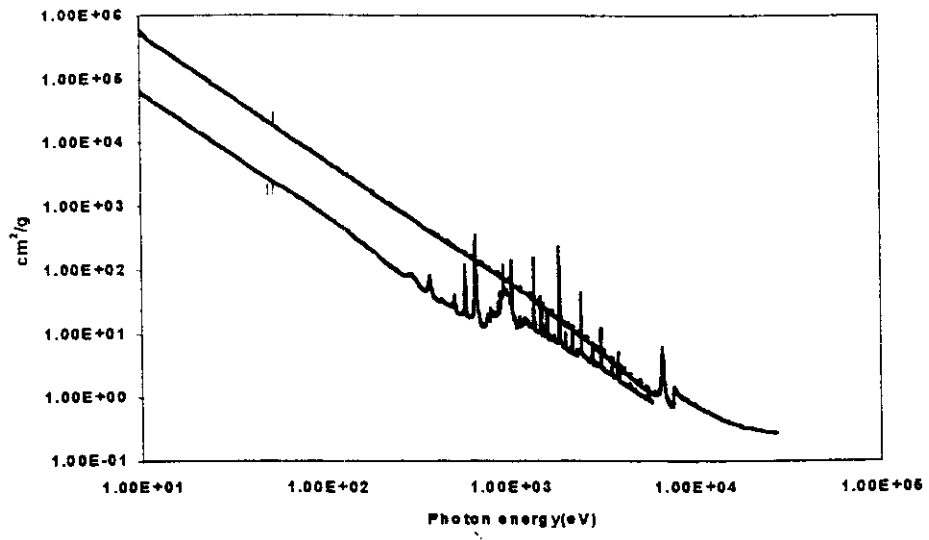

Fig. 7. Photoabsorption cross sections of the solar plasma. I- center of the sun, kT=1362.1 eV, 157.02 g/cc density. II- half-way from the center, r/R_0=0.5545, kT=293.24 eV, 0.7727 g/cc density.

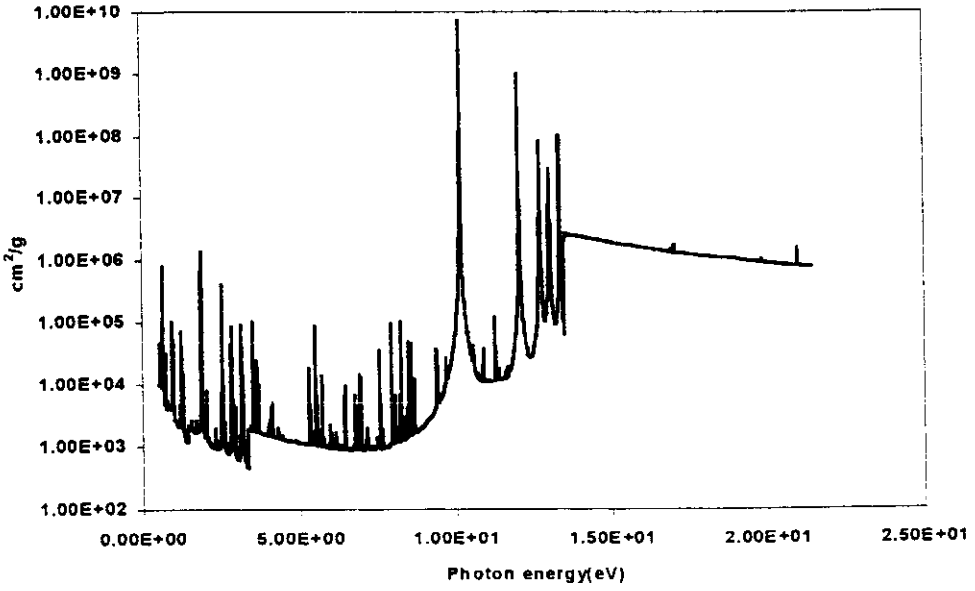

Fig. 8. Photoabsorption cross section near or at the solar surface, kT=1.0724 eV, 9.616×10^{-7} g/cc density, $r\approx R_0$.

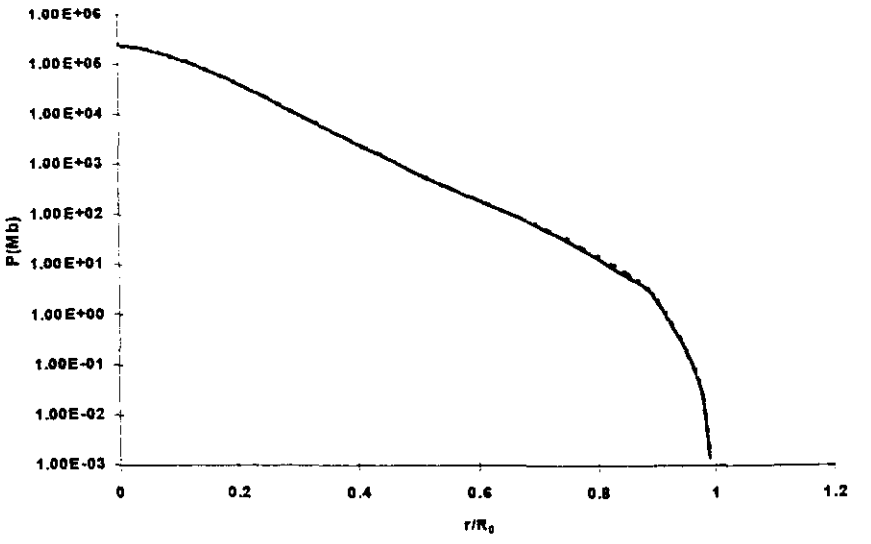

Fig. 9. Solar pressure versus solar radius. The dashed line is given by the standard model, the solid line is this work.

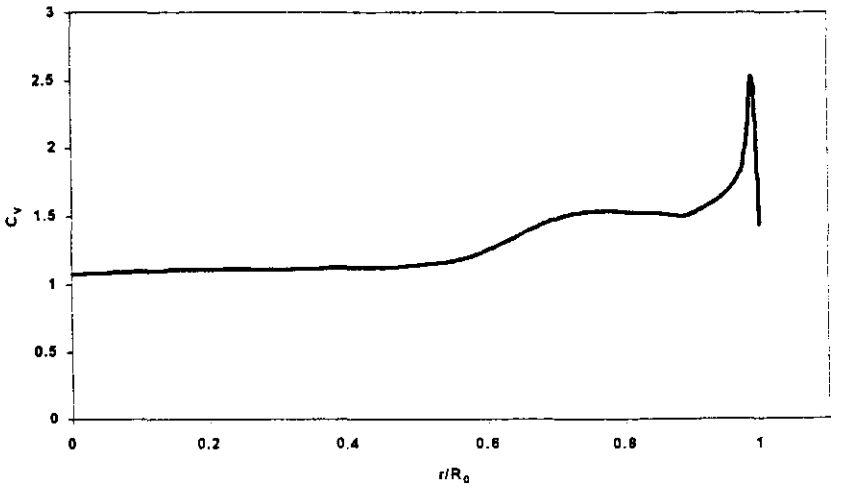

Fig. 10. Specific heat C_V per particle (electrons and nuclei) versus solar radius.

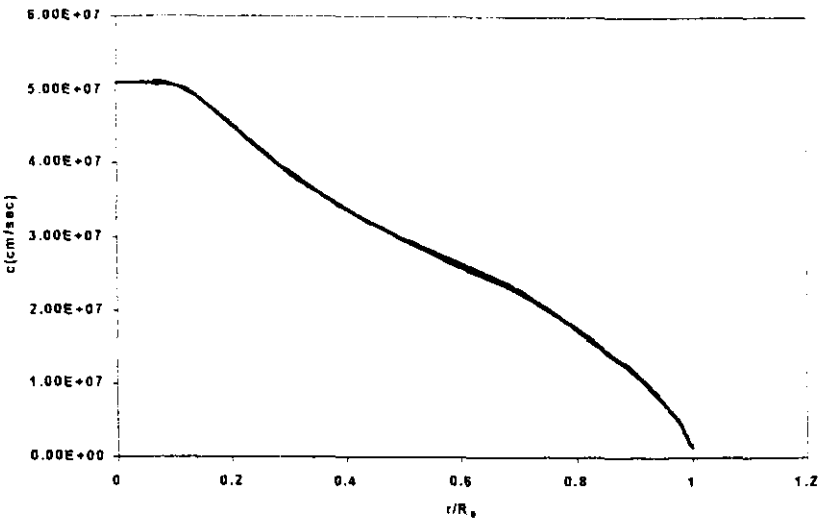

Fig. 11. Speed of sound in the solar plasma versus solar radius. The two solid curves are given by this work and the standard model, the dashed points in between the two solid curves are experimental data.